Glycobiology, 2017, vol. 27, no. 1, 99–109
doi: 10.1093/glycob/cww090
Advance Access Publication Date: 4 October 2016
Original Article

Microbial Biology

Shiga toxin glycosphingolipid receptors and their lipid membrane ensemble in primary human blood–brain barrier endothelial cells

Nadine Legros[2], Stefanie Dusny[3], Hans-Ulrich Humpf[3], Gottfried Pohlentz[2], Helge Karch[2], and Johannes Müthing[1,2,4]

[2]Institute for Hygiene, University of Münster, Robert-Koch-Str. 41, D-48149 Münster, Germany, [3]Institute for Food Chemistry, University of Münster, Corrensstr. 45, D-48149 Münster, Germany, and [4]Interdisciplinary Center for Clinical Research (IZKF), University of Münster, Albert-Schweitzer-Campus 1, D-48149 Münster, Germany

[1]To whom correspondence should be addressed: Tel: +49-251-83 55192; Fax: +49-251-83 55341; e-mail: jm@uni-muenster.de

Received 3 June 2016; Revised 17 August 2016; Accepted 19 August 2016

Abstract

Shiga toxin (Stx)-mediated injury to microvascular endothelial cells in the brain significantly contributes to the pathogenesis of the hemolytic-uremic syndrome caused by enterohemorrhagic *Escherichia coli* (EHEC). Stxs are AB_5 toxins and the B-pentamers of the two major Stx subtypes Stx1a and Stx2a preferentially bind to the glycosphingolipid (GSL) globotriaosylceramide (Gb3Cer) expressed by human endothelial cells. Here we report on comprehensive structural analysis of the different lipoforms of Gb3Cer (Galα4Galβ4Glcβ1Cer) and globotetraosylceramide (Gb4Cer, GalNAcβ3Galα4Galβ4Glcβ1Cer, the less effective Stx receptor) of primary human brain microvascular endothelial cells and their association with *lipid rafts*. Detergent-resistant membranes (DRMs), obtained by sucrose density gradient ultracentrifugation, were used as *lipid raft*-analogous microdomains of the liquid-ordered phase and nonDRM fractions were employed as equivalents for the liquid-disordered phase of cell membranes. Structures of the prevalent lipoforms of Gb3Cer and Gb4Cer were those with Cer (d18:1, C16:0), Cer (d18:1, C22:0) and Cer (d18:1, C24:1/C24:0) determined by electrospray ionization mass spectrometry that was combined with thin-layer chromatography immunodetection using anti-Gb3Cer and anti-Gb4Cer antibodies as well as Stx1a and Stx2a subtypes. Association of Stx receptor GSLs was determined by co-localization with *lipid raft*-specific membrane protein flotillin-2 and canonical *lipid raft* marker sphingomyelin with Cer (d18:1, C16:0) and Cer (d18:1, C24:1/C24:0) in the liquid-ordered phase, whereas lyso-phosphatidylcholine was detectable exclusively in the liquid-disordered phase. Defining the precise microdomain structures of primary endothelial cells may help to unravel the initial mechanisms by which Stxs interact with their target cells and will help to develop novel preventive and therapeutic measures for EHEC-mediated diseases.

Key words: detergent-resistant membranes, glycolipids, *lipid rafts*, lyso-phosphatidylcholine, primary human brain microvascular endothelial cells, sphingomyelin

Introduction

Enterohemorrhagic *Escherichia coli* (EHEC) are the pathogenic subgroup of Shiga toxin (Stx)-producing *E. coli* (STEC). EHEC cause non-bloody and bloody diarrhea, hemorrhagic colitis, thrombotic thrombocytopenic purpura (TTP), and the hemolytic-uremic syndrome (HUS) (Karch et al. 2005; Tarr et al. 2005), severe disorders

characterized by the clinical triad of microangiopathic hemolytic anemia, thrombocytopenia, and acute renal failure (Zoja et al. 2010; Obrig and Karpman 2012). HUS is characterized primarily by glomerular endothelial cell injury resulting in acute renal impairment, while in TTP predominantly injury of human brain microvascular endothelial cells (HBMECs) results in neurological disturbance (Richards and Kavanagh 2009).

The most effective EHEC-derived virulence factors are Stxs of subtype 1a and 2a (Scheutz et al. 2012), which are delivered into the colon. The toxin is then transferred into the circulation, where granulocytes are currently discussed as potential Stx transporters (Brigotti et al. 2013; Carnicelli et al. 2016). Stx1a and Stx2a preferentially bind to the glycosphingolipid (GSL) globotriaosylceramide (Gb3Cer) and to less extent to globotetraosylceramide (Gb4Cer), which are the major GSLs of human endothelial cells of various vascular beds (Müthing et al. 2009; Bauwens et al. 2013 and references therein). HBMECs are widely used to explore the role of this endothelial cell type in cerebral injury according to observed clinical neurological features in TTP (Tsai 2006; Zheng and Sadler 2008), in particular because neurological injury of the brain is the most frequent cause of acute mortality in patients with STEC-HUS (Trachtman et al. 2012).

The Stx B pentamer of the AB_5 toxin binds to the cell surface, followed by internalization of the toxin-GSL complex by various endocytic mechanisms, routing to the endoplasmic reticulum and finally transfer into the cytosol, where the catalytic A1 portion of the A subunit irreversibly inhibits protein biosynthesis at the ribosomes (Sandvig et al. 2010). A growing body of evidence suggests that Stxs (like other ribosome-inactivating proteins) remove adenine moieties not only from rRNA in the cytosol but also efficiently depurinate DNA in the nucleus. This effect leads to DNA damage in cultured cells and is likely to result from direct DNA-damaging activities and/or indirect DNA repair inhibition (Brigotti et al. 2002; Sestili et al. 2005) indicating the existence of more than one retrograde pathway.

Stx receptors are amphipathic GSLs that are built up from a hydrophobic ceramide moiety and a hydrophilic oligosaccharide residue (Levery 2005; Müthing and Distler 2010; Meisen et al. 2011). Their localization in *lipid rafts* in the exofacial leaflet of the plasma membrane makes them excellent candidates as recognition structures for numerous pathogens and bacterial toxins including Stxs (Karlsson 1995; Smith et al. 2004; Hanada 2005). *Lipid rafts* are highly variable membrane microdomains (Klotzsch and Schütz 2013) enriched in cholesterol, sphingomyelin (SM) and GSLs (Róg and Vattulainen 2014) that function not only as platforms in membrane signaling and trafficking (Prinetti et al. 2009; Lingwood and Simons 2010; Simons and Gerl 2010; Komura et al. 2016) but also as adhesion platforms for microorganisms and their toxins (Fujinaga et al. 2003; Teneberg et al. 2004; Lencer and Saslowsky 2005; Gupta and Surolia 2010; Jansson et al. 2010).

So far Stx GSL receptors and their lipid environment have been studied in detail in immortalized HBMECs by us (Schweppe et al. 2008; Betz et al. 2011) and only few studies have been performed so far on the original primary (p) HBMECs, which exhibit a limited life span in vitro. Up to now, not much is known about the expected variability of Stx receptor GSLs regarding their fine structures and possible association with microdomains in pHBMECs (Ramegowda et al. 1999; Eisenhauer et al. 2001; Stricklett et al. 2002; Ergonul et al. 2003; Kanda et al. 2004). Here we report on the comprehensive structural analysis of the various lipoforms of globo-series Stx receptor GSLs isolated from pHBMECs at early cell passages. In addition we will unravel GSL assembly with companion lipids in membrane microdomains employing detergent-resistant membranes (DRMs) as the ruling method to assigning *lipid raft* association (Brown and Rose 1992; Brown 2006; Smith et al. 2006; Lingwood and Simons 2007) providing novel insights into these supramolecular membrane structures of primary human blood–brain barrier endothelial cells.

Results

In this study we first identified globo-series neutral GSLs as potential Stx receptors of pHBMECs using anti-Gb3Cer and anti-Gb4Cer antibodies as well as Stx1a and Stx2a subtypes, which represent the clinically most relevant EHEC-derived toxins. For this purpose we propagated pHBMECs in early passages not beyond passage 7. Although these primary cells were cultivable beyond passage 20, they started to exhibit microscopic signs of senescence and dedifferentiation from passage 10 upwards (Supplementary data, Figure S1). After identification of Stx receptors and structural characterization of their various lipoforms, we analyzed GSL distribution to sucrose gradient fractions obtained by ultracentrifugation and using detergent. This method allows for discrimination of lipids that might be preferentially associated with *lipid rafts* by preparing DRMs (Brown 2006; Lingwood and Simons 2007). DRMs are supposed at least to resemble these microdomain assemblies in cellular membranes being considered and used as *lipid raft*-analogous structures (Morris et al. 2011; Ciana et al. 2014). In addition to GSLs we investigated the distribution of prevalent membrane phospholipids (PLs) to DRM and nonDRM fractions, which may largely represent the liquid-ordered and liquid-disordered phase of membranes, respectively. Analyzed PLs were phosphatidylcholine (PC), lyso-PC and the *lipid raft* marker SM.

Immunodetection of Stx GSL receptors Gb3Cer and Gb4Cer of pHBMECs

GSLs were extracted from in vitro propagated pHBMECs and stained first with orcinol after thin-layer chromatography (TLC) as shown in Figure 1A (lane b) in comparison to reference neutral GSLs from human erythrocytes (lane a). The GSL preparation was then submitted to TLC immunodetection and putative Gb3Cer and Gb4Cer GSLs were verified with anti-Gb3Cer (Figure 1B, lane b) and anti-Gb4Cer antibody (Figure 1C, lane b) when compared to erythrocyte positive Gb3Cer and Gb4Cer controls (Figure 1B, lane a, and Figure 1C, lane a, respectively). pHBMECs were found to express the Stx receptors Gb3Cer and Gb4Cer showing characteristic immunostained double bands for each receptor. This type of doublets suggests highly variable ceramide moieties most likely due to fatty acid heterogeneity, whereby the upper band harbors GSL species with long chain and the lower band those ones with short-chain fatty acids. In addition to the neutral GSLs, an orcinol stain of TLC-separated gangliosides is provided in the Supplementary data, Figure S2 suggesting presence of GM3(Neu5Ac), IV^3Neu5Ac-nLc4Cer and VI^3Neu5Ac-nLc6Cer (not further followed in this study).

Electrospray ionization (ESI) mass spectrometry (MS) of Gb3Cer and Gb4Cer

Exact structures of immunodetected Gb3Cer and Gb4Cer were scrutinized using MS^1 and MS^2 analysis in positive ion mode. The MS^1 overview spectrum (Figure 2A), obtained from three pooled extracts

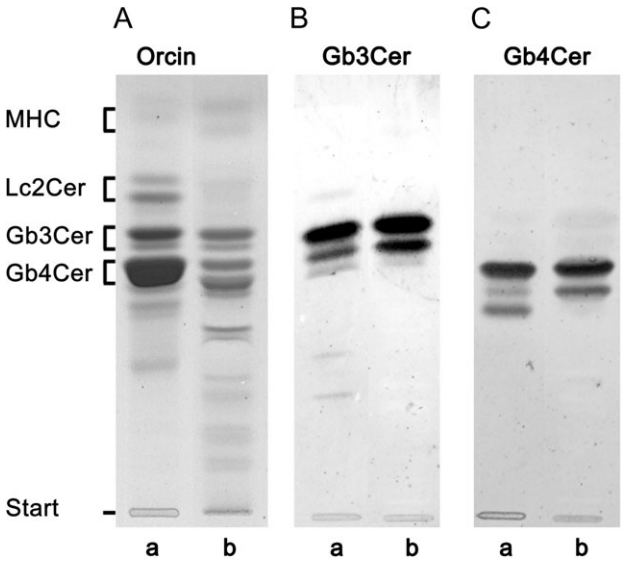

Fig. 1. Antibody- and Stx-mediated detection of Stx receptors in TLC-separated GSL preparations of pHBMECs. (**A**) Orcinol stain, a: 20 μg neutral GSLs of human erythrocytes (R1), b: GSLs corresponding to 1×10^6 cells. (**B**) Anti-Gb3Cer overlay immunodetection, a: 2 μg neutral GSLs of human erythrocytes (R1), b: GSLs corresponding to 2×10^5 cells. (**C**) Anti-Gb4Cer overlay immunodetection, a: 0.2 μg neutral GSLs of human erythrocytes (R1), b: GSLs corresponding to 2×10^5 cells.

by means of preparative TLC of immunostained Gb3Cer doublets (see inset of Figure 2A), indicates the presence of various Gb3Cer lipoforms. Identified structures are Gb3Cer variants carrying sphingosine (d18:1) and a C16:0, C22:0, C24:1, or C24:0 acyl chain in their ceramide moieties according to *m/z* values of $[M+Na]^+$ ions at 1046.64, 1130.74, 1156.76 and 1158.77, respectively (Table I). An example for verification of proposed structures is provided showing an MS^2 spectrum of Gb3Cer (d18:1, C22:0) in Figure 2B together with the corresponding fragmentation scheme (Figure 2C). The fragment ions originating from the monosodiated precursor ions at *m/z* 1130.90 (Figure 2B) are assigned according to the nomenclature of Domon and Costello (1988a,b). Full series of *Y*- and *Z*-type and *B*- and *C*-type ions indicate the sequential loss of the three hexoses from Gb3Cer. In addition, the $^{0,2}A_2$- and $^{0,2}A_3$-ions, produced by ring cleavages, and the W^{II}-ions, indicators for sphingosine (4-sphingenine, d18:1), give rise to the complete structure of Gb3Cer (d18:1, C22:0).

The MS^1 spectrum of Gb4Cer twin bands was obtained in the same manner as that one of Gb3Cer and is shown in Figure 3A, supplemented with the inset of an immunostained Gb4Cer doublet. The overview spectrum indicates existence of several different Gb4Cer lipoforms with sphingosine (d18:1) and C16:0, C22:0, C24:1 or C24:0 fatty acid residues in their ceramide portions, leading to *m/z* values of the corresponding sodiated species at 1249.77, 1333.87, 1359.90 and 1361.90, respectively (Table I). The MS^2 spectrum (Figure 3B) together with the explanatory fragmentation scheme exemplarily shows the fine structural analysis of Gb4Cer (d18:1, C16:0) (Figure 3C). Full series of *B*- and *Y*-type ions, indicating the sequential loss of one *N*-acetylated hexosamine and three hexoses from Gb4Cer, and the W^{II}-ions, which again hint at the presence of sphingosine (4-sphingenine, d18:1) in the ceramide moiety, give rise to the complete structure of Gb4Cer (d18:1, C16:0).

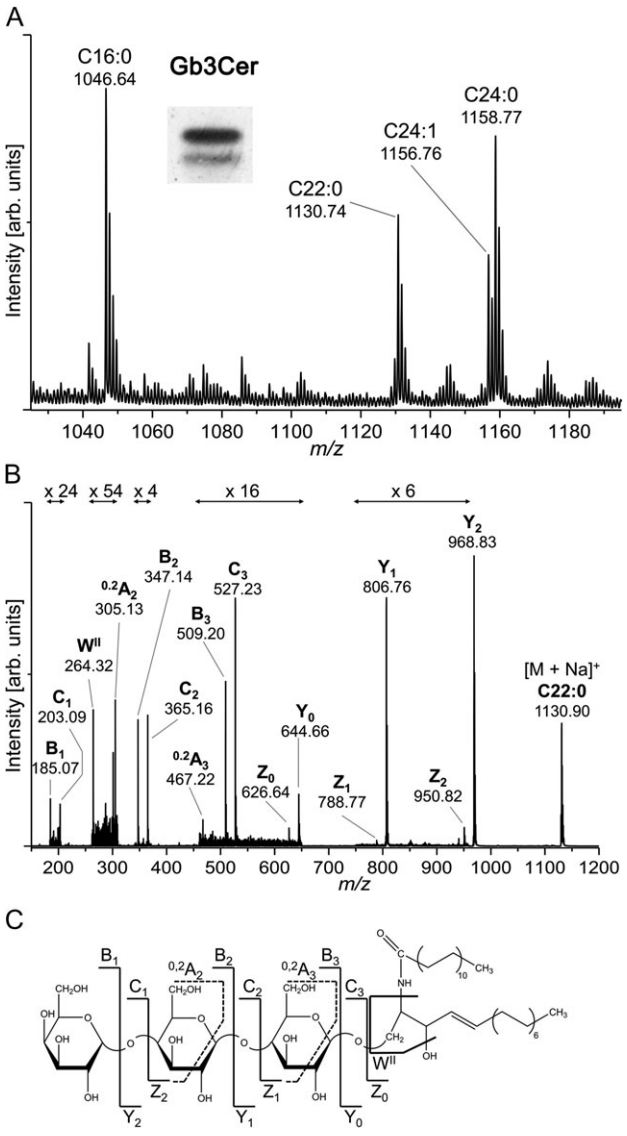

Fig. 2. Mass spectrometric identification of Gb3Cer lipoforms of pHBMECs. (**A**) MS^1 spectrum of Gb3Cer species, obtained after preparative TLC from the pooled extracts of three TLC immunostains (see Figure 1B, lane b) and recorded as $[M+Na]^+$ ions in the positive ion mode. The inset indicates the antibody-positive bands from which the silica gel extracts were prepared. Ion species corresponding to Gb3Cer lipoforms with invariable sphingosine (d18:1) and varying fatty acids (C16:0, C22:0, C24:1, or C24:0) are labeled in the spectrum. The major $[M+Na]^+$ ions of the detected Gb3Cer variants and their proposed structures are listed in Table I. (**B**) MS^2 spectrum of Gb3Cer (d18:1, C22:0) of pHBMECs and (**C**) corresponding auxiliary fragmentation scheme.

Association of Gb3Cer and Gb4Cer with *lipid raft*-analogous microdomains

Western blot analysis of flotillin-2, a microdomain scaffolding and *lipid raft*-associated protein of mammalian cells (Head et al. 2014), revealed preferred localization in DRMs according to predominance in canonical DRM fraction F2 as shown in Figure 4A. An additional Western blot, obtained from a second independent biological replicate of pHBMECs, corroborates the *lipid raft* association of flotillin-2 (Supplementary data, Figure S3A). Slightly enhanced occurrence of Gb3Cer in DRM fractions (F1–F3) with relative contents of 54%

Table I. Proposed structures of Stx receptors Gb3Cer and Gb4Cer of pHBMECs determined by mass spectrometry

m/z_{exp}	GSL lipoforms
1158.77	Gb3Cer (d18:1, C24:0)
1156.76	Gb3Cer (d18:1, C24:1)
1130.74	Gb3Cer (d18:1, C22:0)
1046.64	Gb3Cer (d18:1, C16:0)
1361.90	Gb4Cer (d18:1, C24:0)
1359.90	Gb4Cer (d18:1, C24:1)
1333.87	Gb4Cer (d18:1, C22:0)
1249.77	Gb4Cer (d18:1, C16:0)

GSLs were obtained after immunodetection with Gb3Cer- and Gb4Cer-specific antibodies using preparative TLC (see overview spectra in Figures 2A and 3A, respectively) and analyzed as $[M+Na]^+$ ions in the positive ion mode by MS^1 and MS^2. Examples of MS^2 spectra of Gb3Cer (d18:1, C22:0) and Gb4Cer (d18:1, C16:0) are given in Figures 2B and 3B, respectively.

in the first replicate (Figure 4B) and 48% in the second replicate (Supplementary data, Figure S3B) indicates prevalence of the high-affinity receptor of Stxs in the liquid-ordered phase of membranes. However, relative contents of Gb3Cer amounting to 17% and 24% in the intermediate fractions (F4–F6) and 29% and 28% in the bottom fractions (F7 and F8) of replicate 1 and 2 shown in Figure 4B and the Supplementary data, Figure S3B, respectively, provide evidence for occurrence of Gb3Cer in the liquid-disordered phase as well. Nevertheless, data of both biological replicates of pHBMECs substantiates the association of Gb3Cer with *lipid rafts* and its preferred occurrence in a microdomain environment.

A somewhat lower relative content of 38% was determined for Gb4Cer in DRM fractions (F1–F3) of replicate 1, accompanied by 32% in the intermediate fractions (F4–F6) and 30% in the bottom fractions (F7 and F8) as demonstrated in Figure 4C. A shift to somewhat higher content of 50% was observed for Gb4Cer in DRM fractions (F1–F3) of replicate 2 with complementary 26% in intermediate fractions (F4–F6) and 24% in the bottom fractions (F7 and F8) as shown in the Supplementary data, Figure S3C. These results gave evidence for an on overage little less strong association of Gb4Cer with membrane microdomains and subtly enhanced Gb4Cer content in the liquid-disordered phase, indicative for less marked but notable association with *lipid rafts*.

The total amounts of Gb3Cer and Gb4Cer were roughly calculated from TLC immunopositive bands of DRM and nonDRM fractions corresponding to 4×10^5 cells. This was done using a neutral GSL preparation of human erythrocytes with well-known concentrations of globo-series GSLs serving as reference. Obtained Gb3Cer amounts for sucrose gradient fractions of pHBMECs were 0.2 µg in the DRM fractions (F1–F3) and 0.1 µg each in the intermediate fractions (F4–F6) and the bottom fractions (F7 and F8) as an approximate average value for both replicates. The Gb4Cer quantities were somewhat lower but in the same order of magnitude with 0.1 µg in the DRM fractions and 0.06 µg each in the intermediate fractions (F4–F6) and the bottom fractions (F7 and F8) representing an approximate average amount for both replicates.

In order to verify specific binding of Stx1a and Stx2a to the antibody-detected globo-series GSLs, TLC overlay assays were performed with the same preparations of gradient fractions but employing Stx1a and Stx2a. Chromtograms were overlayed with Stx1a and Stx2a and bound GSLs were visualized with anti-Stx1 and anti-Stx2 antibody, respectively, combined with appropriate secondary AP-conjugated antibodies. Stx1a exhibited strongest positive reaction

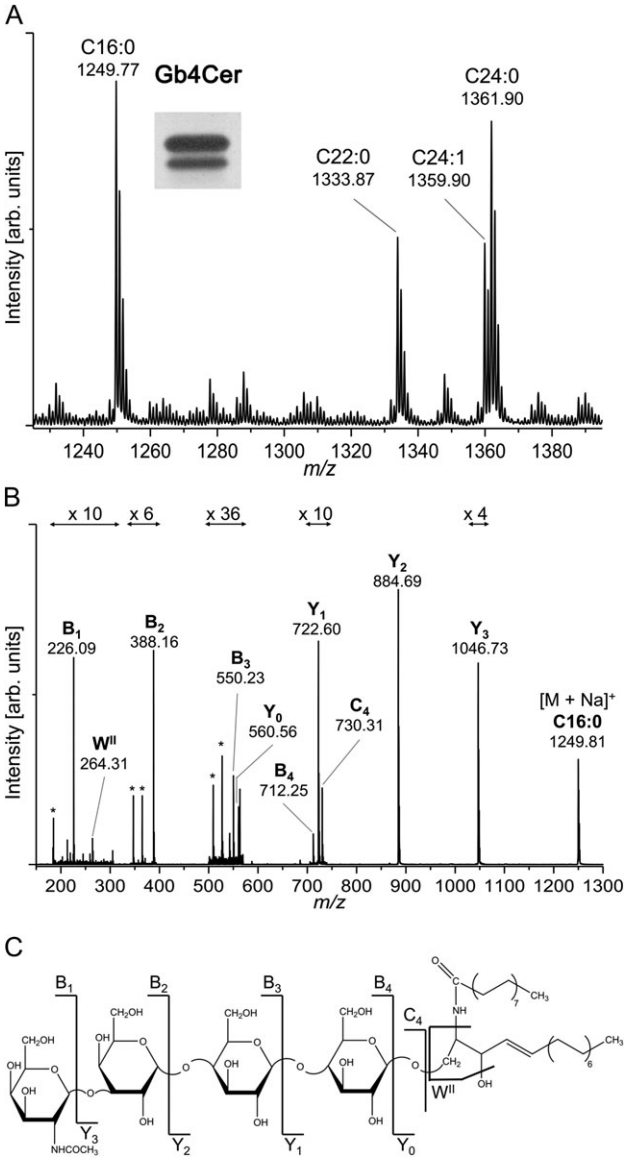

Fig. 3. Mass spectrometric identification of Gb4Cer lipoforms of pHBMECs. (**A**) MS^1 spectrum of Gb4Cer species, obtained after preparative TLC from the pooled extracts of three TLC immunostains (see Figure 1C, lane b) and recorded as $[M+Na]^+$ ions in the positive ion mode. The inset indicates the antibody-positive bands from which the silica gel extracts were prepared. Ion species corresponding to Gb4Cer lipoforms with invariable sphingosine (d18:1) and varying fatty acids (C16:0, C22:0, C24:1, or C24:0) are marked in the spectrum. The major $[M+Na]^+$ ions of the detected Gb4Cer variants and their proposed structures are listed in Table I. (**B**) MS^2 spectrum of Gb4Cer (d18:1, C22:0) of pHBMECs and (**C**) corresponding auxiliary fragmentation scheme.

with Gb3Cer in DRM fraction F2 (Figure 5A) and showed a very similar double band pattern as obtained in the antibody-mediated TLC overlay assay (Figure 4B), although being less sensitive when compared to anti-Gb3Cer immunodetection as known from previous binding assays (Meisen et al. 2005; Schweppe et al. 2010). While Stx1a did not interact with Gb4Cer (Figure 5A), Stx2a showed, in addition to preponderant binding towards Gb3Cer, recognizable adhesion to Gb4Cer as shown in Figure 5B for the parallel to Stx1a performed Stx2a TLC overlay assay using identical

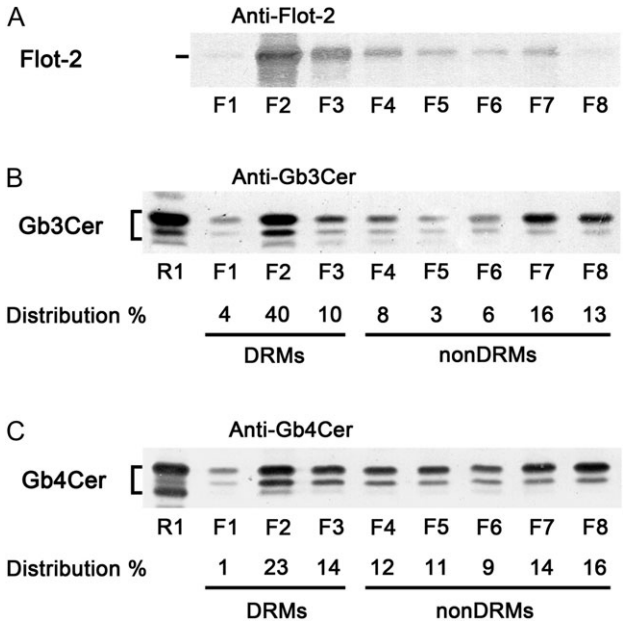

Fig. 4. Detection of flotillin-2 and globo-series GSLs Gb3Cer and Gb4Cer in sucrose density gradient fractions of pHBMECs. (**A**) Western blot detection of flotillin-2 in a protein preparation after SDS-PAGE separation. (**B**) TLC immunodetection of Gb3Cer with anti-Gb3Cer antibody and (**C**) TLC immunodetection of Gb4Cer with anti-Gb4Cer antibody. The protein preparation (**A**) corresponds to 1×10^6 cells; the GSL extracts used for detection of Gb3Cer (**B**) and Gb4Cer (**C**) correspond to 4×10^5 cells, respectively. Amounts of applied reference neutral GSLs from human erythrocytes (R1) were 2 μg for anti-Gb3Cer (**B**) and 0.2 μg for anti-Gb4Cer overlay assay (**C**).

gradient fractions. A second overlay approach from a further biological replicate of pHBMECs corroborated the binding features of Stx1a and Stx2a as shown in the Supplementary data, Figures S4A and B, respectively. The comparable binding patterns obtained in case of the DRM F2 fractions with anti-Gb3Cer antibody on the one hand and with Stx1a and Stx2a on the other hand suggest that the binding affinity of both Stxs does not depend on the ceramide composition. Since the fatty acid chain length does not significantly influence the binding, the oligosaccharide structure seems to be the major epitope recognized by the toxin in TLC overlay binding assays.

In addition to the MS^1 and MS^2 spectra of Gb3Cer and Gb4Cer species from total GSLs (Figures 2 and 3, respectively) we provide MS^1 and MS^2 spectra of Gb3Cer and Gb4Cer from F2 (DRM) and F7 (nonDRM) fractions in the Supplementary data. The Gb3Cer overview mass spectra of the F2 and F7 fractions are shown in the Supplementary data, Figures S5 and S6, respectively, each accompanied by an MS^2 spectrum of a randomly selected Gb3Cer species and an explanatory fragmentation scheme. The relative increase observed for the signal intensity of the ions corresponding to Gb3Cer (d18:1, C24:1) and the concomitant decrease of Gb3Cer (d18:1, C24:0) intensity in the nonDRM F7 fraction indicates a notable difference when compared to the DRM F2 fraction, suggesting a slight preference of Gb3Cer with C24:1 fatty acid for the liquid-disordered phase of the plasma membrane. In addition to Gb3Cer spectra, Gb4Cer overview mass spectra of the F2 and F7 fractions are shown in the Supplementary data, Figures S7 and S8, respectively, each accompanied by an MS^2 spectrum of a randomly chosen Gb4Cer species and a descriptive fragmentation scheme. The comparison of both spectra did not reveal significant differences regarding Gb4Cer variability.

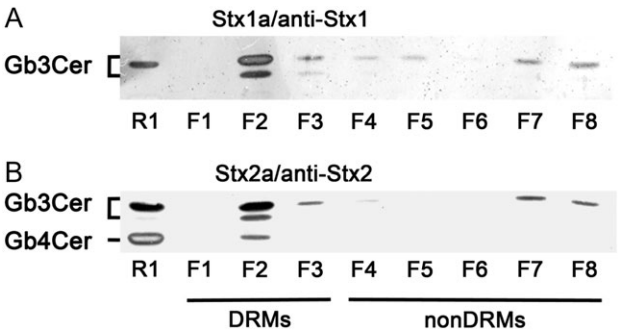

Fig. 5. Detection of Stx-binding GSLs in sucrose density gradient fractions of pHBMECs. (**A**) TLC overlay assay detection of Stx1a- and (**B**) Stx2a-binding GSLs using Stx1- and Stx2-specific antibody, respectively. GSL extracts correspond to 8×10^5 cells and 2 μg of reference neutral GSLs from human erythrocytes (R1) were applied in each assay.

However, co-extracted impurities detectable along with the GSLs in the spectra of DRM F2 and nonDRM F7 fractions and disturbing the spectra presentations might derive from the silica gel and/or remnants of Triton X-100 detergent in the gradient fractions.

SM and lyso-PC are specific markers for DRM and nonDRM fractions, respectively

PC was found to distribute almost equally to DRM fraction F2 and nonDRM bottom fraction F7, each flanked by lower quantities of PC in adjacent fractions F3 and F8, respectively, indicating no particular enrichment in the liquid-ordered or liquid-disordered phase of the membranes (Figure 6). Importantly, SM could be identified as unequivocal *lipid raft* marker, which appeared solely in the DRM fractions with obvious prevalence in canonical DRM fraction F2 as highlighted with an arrow head in Figure 6. On the other hand, SM was undetectable in nonDRM fractions, whereby lyso-PC appeared only in the bottom fractions F7 and F8, marked with an arrow head in the TLC lane of fraction F7 (Figure 6). This distribution identifies lyso-PC as a specific marker of the liquid-disordered phase, requiring structural verification as provided by MS analysis in the next chapter.

MS profiles of PLs in DRMs and nonDRMs

Classical DRM fraction F2 and typical nonDRM fraction, that is bottom fraction F7, from sucrose gradients were submitted to ESI MS and the resulting MS^1 spectra are shown in Figure 7A for F2 and in Figure 7B for F7, in which the signals of protonated $[M+H]^+$ molecules are marked with *m/z* values. Several SM lipoforms, highlighted by grayed boxes, were found to harbor sphingosine (d18:1) and a fatty acid, ranging from C14:0 to C26:0, and were identified as DRM-specific (and thus most likely *lipid raft*-associated) structures in fraction F2. Notably, SM (d18:1, C16:0) with short chain and SM (d18:1, C24:2/C24:1/C24:0) with long-chain fatty acyl residues were the dominant SM variants, accompanied by minor SM (d18:1, C14:0) and minute SM (d18:1, C26:2/C26:1/C26:0). SM lipoforms with C18, C20, or C22 fatty acids were not found in the lipid extract of the F2 fraction. As supposed from TLC identification of PLs (Figure 6), various PC species appeared as highly abundant $[M+H]^+$ signals, namely PC (32:0) and PC (34:1), flanked by $[M+Na]^+$ ions of PC (34:1) and PC (34:0) [corresponding to number 6 and 7, respectively, in the MS^1 spectrum], and last not least the most abundant $[M+H]^+$ ions of PC (36:2) and PC (36:1). The peaks of minor protonated and monosodiated

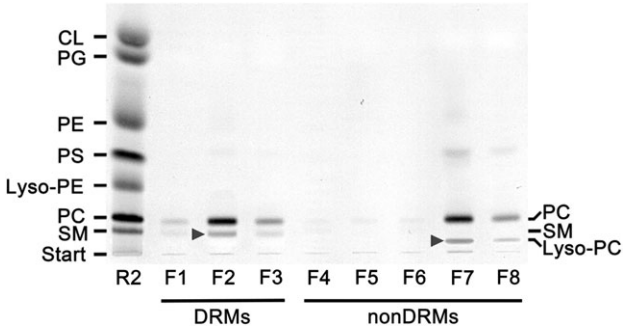

Fig. 6. Identification of PLs in sucrose density gradient fractions of pHBMECs. PLs of gradient fractions F1–F8, corresponding to 2×10^6 cells, were stained after TLC separation with molybdenum blue. They were matched to a PL reference mixture (R2) containing (from top) cardiolipin (CL), phosphatidylglycerol (PG), PE, phosphatidic acid (PA), lyso-PE, PC and SM. SM is marked with an arrow head in fraction F2 and lyso-PC with an arrow head in F7, indicating their preferential presence in canonical DRM fraction F2 and typical nonDRM bottom fraction F7, respectively.

molecules, which could be assigned to phosphatidylethanolamine (PE) and triglyceride (TG) species, are denoted with numbers (PE, 1–4; TGs, 8–15) and itemized in the legend of Figure 7A.

The MS^1 profile of nonDRM bottom fraction F7, in which the peaks of protonated $[M+H]^+$ lipid species are denoted with *m/z* values, shows some significant differences regarding specific diminishment of monounsaturated PC (32:1), a slight increase in saturated to threefold unsaturated PC (36) and two- to fourfold unsaturated PC (38) species [corresponding to number 10–13 and number 14–16, respectively, in the MS^1 spectrum], absence of TGs, and complete lack of any SM species (Figure 7B). However, as most prominent distinction, specific enrichment of lyso-PC variants, which are emphasized by grayed boxes in the spectrum, was observed. Lyso-PC (18:1), accompanied by less abundant lyso-PC (16:0) and minor lyso-PC (16:1), were identified in nonDRM bottom fraction F7, which were undetectable in the F2 DRM fraction and can be considered as a reliable PL species of the liquid-disordered membrane phase of pHBMECs. Minor protonated and monosodiated PE (number 1–3 and number 7–9, respectively) and monosodiated PC species (number 4–6 and number 10–16) are itemized in the legend of Figure 7B.

In order to rule out any doubts about the correctness of MS analyses especially of low abundance PLs, MS^2 spectra of minor SM species of DRM fraction F2 and low abundant lyso-PC of nonDRM fraction F7 are displayed as Supplementary data. SM (d18:1, C14:0) and SM (d18:1, C26:2) (see overview spectrum in Figure 7A) were chosen as random examples for low abundance and the MS^2 spectra obtained from precursor ions at *m/z* 675.52 and *m/z* 839.63 together with the corresponding CID fragmentation schemes are shown in the Supplementary data, Figure S9A and B, respectively. The CID spectra of SM minorities clearly indicate the potential to differentiate between sphingosine base and *N*-acyl fatty acid, i.e. allowing for discrimination of possible SM species with Cer (d18:1, C14:0) or Cer (d18:0, C14:1). As an example of a low abundant lyso-PC species (see overview spectrum in Figure 7B), the MS^2 spectrum of lyso-PC (16:1) derived from precursor ions at *m/z* 494.33 was chosen and is shown in the Supplementary data, Figure S10, together with the related fragmentation scheme. In conclusion, MS^2 analysis of minor lipid species, almost hidden in the noise of the spectra, allows for corroboration of the MS^1-based structural proposals of PLs occurring in minute quantities in DRM and nonDRM samples.

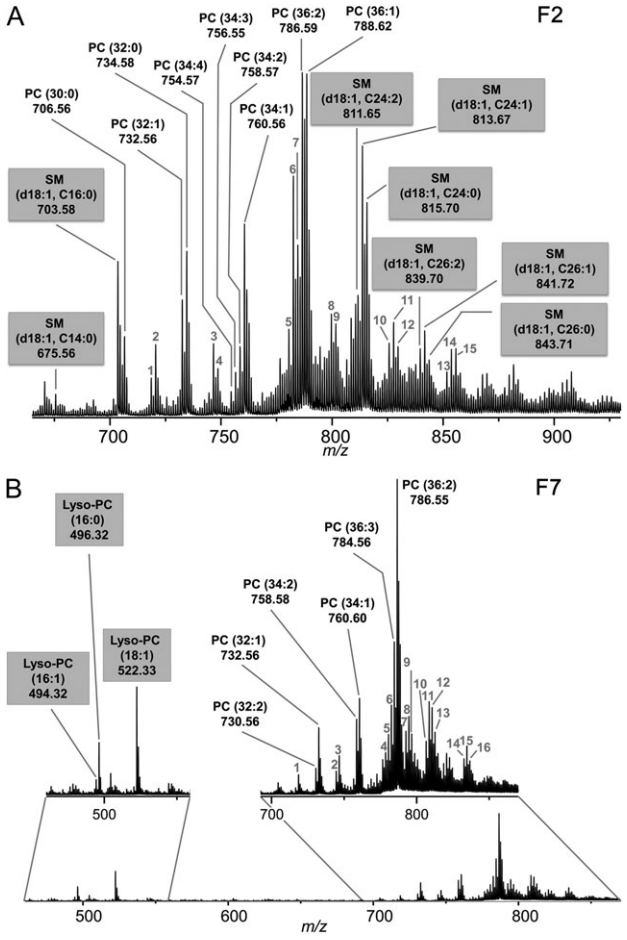

Fig. 7. MS^1-spectra of PLs of DRM fraction F2 (**A**) and nonDRM fraction F7 (**B**) recorded in the positive ion mode. The assigned PC and SM species (**A**) represent the protonated molecules, whereby SM variants as markers of the liquid-ordered membrane phase (*lipid rafts*) are highlighted as grayed boxes. Ions denoted with numbers are (i) $[M+H]^+$ ions of PEs with *m/z* 718.59 (34:1), 720.58 (34:0), 746.61 (36:1) and 748.61 (36:0) with numbers 1–4, (ii) $[M+Na]^+$ ions of PCs with *m/z* 780.57 (34:2), 782.59 (34:1) and 784.60 (34:0) with numbers 5–7 and (iii) $[M+Na]^+$ ions of TGs with *m/z* 799.67 (46:1), 801.68 (46:0), 825.72 (48:2), 827.72 (48:1), 829.70 (48:0), 851.70 (50:3), 853.73 (50:2) and 855.74 (50:1) with numbers 8–15. The assigned PC and lyso-PC species (**B**) represent the protonated molecules, whereby lyso-PC variants as markers of the liquid-disordered membrane phase are highlighted as grayed boxes. Ions denoted with numbers are (i) $[M+H]^+$ ions of PEs with *m/z* 718.59 (34:1), 744.56 (36:2) and 746.56 (36:1) with numbers 1–3, (ii) $[M+Na]^+$ ions of PCs with *m/z* 778.55 (34:3), 780.53 (34:2) and 782.54 (34:1) with numbers 4–6, (iii) $[M+Na]^+$ ions of PEs with *m/z* 792.56 (38:3), 794.59 (38:2) and 796.59 (38:1) with numbers 7–9 and (iv) $[M+Na]^+$ ions of PCs with *m/z* 806.58 (36:3), 808.58 (36:2), 810.60 (36:1), 812.58 (36:0), 832.58 (38:4), 834.60 (38:3) and 836.58 (38:2) with numbers 10–16.

Discussion

Thrombotic microangiopathy observed in EHEC infections is characterized by thrombosis formation in the microvasculature of various organs resulting in the HUS and TTP (Nangaku et al. 2007). HUS and TTP are caused by Stx-mediated injury of the microvascular endothelium (Bielaszewska and Karch 2005) and renal and neurological involvement are typical for EHEC-caused infections, indicating the kidney and the brain as the two primary target organs in humans (Trachtman et al. 2012). While in HUS primarily

glomerular endothelial cell injury results in acute renal impairment, in TTP damage of brain microvascular endothelial cells results in neurological disturbance (Richards and Kavanagh 2009) being the most frequent cause of acute mortality in patients suffering from severe EHEC infections (Trachtman et al. 2012). Investigations on Stx receptors of immortalized HBMECs performed in the past by our laboratory (Schweppe et al. 2008; Betz et al. 2011) revealed Gb3Cer (d18:1, C16:0) and Gb3Cer (d18:1, C24:1/C24:0) as the predominant Stx GSL receptors of the endothelial cell line. Its Gb3Cer profile was similar to that one determined for pHBMECs in this study, indicating only a little difference in the intensity of the MS signal for Gb3Cer (d18:1, C22:0), which was found to be more abundant in pHBMECs (Figure 2A) when compared to immortalized HBMECs (Schweppe et al. 2008).

First evidence for expression of globo-series neutral GSLs as functional receptors for Stxs in pHBMECs came from investigations working on the effects of cytokines as sensitizing agents for pHBMECs (Eisenhauer et al. 2001, 2004; Stricklett et al. 2002; Ergonul et al. 2003). Subsequent preliminary structural analyses regarding GSL expression of pHBMECs gave hints on the presence of Gb3Cer and Gb4Cer as major neutral GSLs, harboring sphingenine (=sphingosine) and fatty acid with variable chain lengths in their ceramide moieties (Kanda et al. 2004). We now close this gap of knowledge with a comprehensive structural characterization of Stx receptors Gb3Cer and Gb4Cer of pHBMECs and, moreover, provide a fine analysis on the lipid environment of these functionally important GSLs in the liquid-ordered and the liquid-disordered phase of the plasma membrane of pHBMECs. For this purpose we prepared DRM and nonDRM fractions as corresponding equivalents for *lipid raft* microdomains and non-*lipid raft* areas, respectively, a technology that still represents the ruling method for assigning lipid and protein raft affinity (Brown 2006; Lingwood and Simons 2007). By doing so, we could show co-localization of Gb3Cer and Gb4Cer with SM in the liquid-ordered membrane phase of pHBMECs, represented by sucrose gradient fractions F1–F3.

When compared with immortalized HBMECs (Betz et al. 2011), the association of Gb3Cer and Gb4Cer with supramolecular membrane microdomains was found to be less strict in case of pHBMECs. Interestingly, lipoforms of SM with C16 and C24 fatty acid detected in pHBMECs correlated with ceramide heterogeneity of Gb3Cer and Gb4Cer, which both exhibited a similar lipid anchor variability with prominent Cer (d18:1, C16:0) and Cer (d18:1, C24:1/C24:0). With regard to specific occurrence of marker lipids in the different membrane phases, monotailed lyso-PC could be clearly identified as a specific marker of the liquid-disordered phase due to its exclusive presence in the nonDRM fractions F7–F8 of pHBMEC membranes.

Lipid rafts are transient nanometric to submicrometric assemblies that can be stabilized into signaling platforms, which, for example, dynamically interact with the cytoskeleton in response to extracellular stimuli, regulate membrane turnover and adherence to the extracellular matrix and are sites of cellular entry of certain pathogens and toxins (Simons and Gerl 2010; Head et al. 2014; Carquin et al. 2015; Sonnino et al. 2015). *Lipid rafts* represent well accepted supramolecular plasma membrane structures, which are exploited by pathogens as adhesion platforms during the initial event in host-pathogen interaction (Vieira et al. 2010). GSLs, that are localized with surface-exposed oligosaccharides in the outer leaflet of the plasma membrane, may act as specific entry platforms for many pathogens and their toxins such as Stx, cholera toxin and other related AB_5-subunit toxins (Lencer and Saslowsky 2005; Chinnapen et al. 2007). In particular, the presence of Gb3Cer receptor GSLs of Stx in *lipid rafts* is believed to play a key role in the pathology of HUS (Lingwood et al. 2010). The fatty acid heterogeneity of the ceramide lipid anchor may be of functional importance in the adhesion process of Stxs based on the various lipoforms of Gb3Cer and their different interaction with other *lipid raft*-associated membrane constituents in ordered microdomains. Most importantly, the embedding of Gb3Cer into *lipid rafts* seems to be essential to the pathology of HUS as shown by immunohistological investigations of human kidney sections (Khan et al. 2009). Collectively, association of GSL receptors with domains in the liquid-ordered phase of the plasma membrane is believed to be a general requirement for efficient binding and subsequent internalization to intracellular targets. However, the impact of membrane assembly of GSLs in *lipid rafts* of pHBMECs and their functional role in Stx-mediated brain injury through damaging those endothelial cells, which make up the blood–brain barrier, remain elusive and pose new questions on this topic.

At present, microvascular kidney and brain endothelial cells are considered to be the preferential direct cellular targets of Stxs derived from EHEC (Bielaszewska and Karch 2005; Richards and Kavanagh 2009; Zoja et al. 2010; Obrig and Karpman 2012; Bauwens et al. 2013). Evidence for a direct effect of Stx on renal tubular epithelium came from studies performed in a suitable murine model (Porubsky et al. 2014). Mice do express Stx receptor Gb3Cer, like humans, in the tubular epithelium, but do not express Gb3Cer in glomerular endothelial cells thus explaining why mice are free of glomerular thrombotic microangiopathy. However, it could be shown by Porubsky and co-workers that direct acute tubular damage contributes to Stx-mediated kidney failure (Porubsky et al. 2014). This adds a further facet to the complex history of extraintestinal complications by direct action of Stx on renal epithelial cells in addition to cells of the microvasculature of brain and kidney. With regard to novel developments of Stx neutralizers it should be a relatively easy task to produce glycan-functionalized nontoxic gold or diamond nanoparticles bearing the Gb3 trisaccharide (Chien et al. 2008; Mochalin et al. 2012; Barras et al. 2013) in order to neutralize Stx1a as well as Stx2a in cell cultures using kidney endothelial and epithelial cells or in animal models.

Often mentioned in the literature, an indirect action of Stx seems to be the plausible reason for the onset of hemolytic anemia. Platelets participate in narrowing of blood vessels and partial occlusion of microvessels by forming thrombi, most likely with the involvement of Stx which is known to bind to platelets via Gb3Cer being expressed by human platelets (Cooling et al. 1998; Ghosh et al. 2004). The reasonable explanation for microangiopathic hemolytic anemia is that shear stress occurring by squeezing through partly occluded vessels might cause mechanical disruption of erythrocytes, which in turn results in reduction of number and fragmentation of red blood cells in patients suffering from EHEC infections (Nangaku et al. 2007; Richards and Kavanagh 2009). We therefore questioned in a very recent study whether a direct damage of developing erythrocytes might be the cause or at least contribute to anemia during HUS (Betz et al. 2016). Based on an ex vivo cell propagation system of human $CD34^+$ stem cells, we were able to demonstrate that Stx is capable of direct injury of erythrocytes at certain developmental stages of erythropoiesis namely poly- and orthochromatic erythroblasts (Betz et al. 2016). This data suggests, albeit somewhat speculative at this stage of research, that Stx-mediated damage of erythrocyte progenitor cells in the bone marrow

may contribute to anemia observed in EHEC-caused extraintestinal complications and furthermore explains the huge demand of blood transfusion during onset of HUS.

Conclusions

We believe that increasing knowledge on the complex fine architecture of the endothelial plasma membrane and understanding the sophisticated microbial strategies, which pathogenic bacteria have developed throughout evolution to overcome cellular membrane barriers in the mammalian organism, will contribute to the development of novel human strategies in the fight against infectious diseases. Novel oligosaccharide mimetics directed at neutralization of toxins' cytotoxic activity are challenging compounds to block toxin binding and subsequent cellular internalization (Sharon 2006).

Materials and methods

Cultivation of pHBMECs

Primary human brain microvascular endothelial cells (pHBMECs) were obtained from ScienCell™ (Carlsbad, CA, USA; Cat. No. 1000), where "p" stands for "primary" to discriminate the cell type of this study from previous work on immortalized endothelial cells or endothelial cell lines (Bauwens et al. 2011; Betz et al. 2011). Cryopreserved cells from the 1st passage were thawed, propagated at 37°C in a humidified atmosphere containing 5% CO_2 in air in endothelial cell medium (ECM) with supplements [5% fetal bovine serum, 1% endothelial cell growth supplement and 1% penicillin/streptomycin solution (ECM, ScienCell™, Cat. No. 1001)]. The cells were cultured until 90% confluence and then passaged by trypsinization using 0.25% Trypsin-EDTA (Invitrogen, Karlsruhe, Germany; cat. 25,200) following established protocols (Bauwens et al. 2011; Betz et al. 2011). pHBMECs of the 4th passage were used for establishing a master bank stored at −192°C in the gas phase of liquid nitrogen. In order to produce sufficient cell material for lipid analyses, a vial of the master bank (5×10^5 cells) was thawed and cells were propagated in 175 cm^2 tissue culture flasks (Greiner Bio-One, Frickenhausen, Germany) in ECM without antibiotics not exceeding passage 8. Growth behavior and morphological features of pHBMECs were controlled microscopically with respect to signs of senescence and dedifferentiation being typical for primary cells after long time cultivation (Supplementary Figure S1). Cells were continuously controlled using an Axiovert 40 C microscope (Carl Zeiss AG, Oberkochen, Germany) and monitored with a digital camera (Canon PowerShot G10, Canon, Tokyo, Japan), documented with AxioVison 4.8 (Zeiss) and processed with Adobe Photoshop software (Adobe Systems, San Jose, CA, USA).

Stx1a and Stx2a

Stx1a and Stx2a (in previous publications referred to as Stx1 and Stx2, now changed to Stx1a and Stx2a following the recommendations of Scheutz et al. (2012) for correct nomenclature) were purified from *E. coli* C600(H19J) carrying the stx_1 gene from *E. coli* O26:H11 strain H19 (Smith and Linggood 1971) and from *E. coli* C600(933 W) carrying the stx_2 gene from *E. coli* O157:H7 strain EDL933 (Strockbine et al. 1986), respectively, as previously described (Bauwens et al. 2011). Purity of the Stx1a and Stx2a preparations was monitored by SDS-PAGE, and the structural integrity of both toxins was checked by peptide mapping employing MS (Müthing et al. 2009).

Isolation of GSLs from pHBMECs

Lipids were isolated from confluent cell layers grown in 175 cm^2 tissue culture flasks (Greiner Bio-One) using methanol as the first extraction solvent (Betz et al. 2011; Storck et al. 2012). The methanolic slurry was centrifuged and the sediment was extracted successively with chloroform/methanol (1/2, v/v), chloroform/methanol (1/1, v/v) and chloroform/methanol (2/1, v/v). The supernatants were pooled, dried by rotary evaporation, and co-extracted alkaline-labile PLs and TGs were removed by mild saponification. After dialysis, dried extracts were dissolved in chloroform and applied to a small silica gel 60 column (2 g). Impurities were removed with chloroform/methanol (99/1, v/v) and chloroform/methanol (98/2, v/v) and GSLs were eluted with chloroform/methanol (1/2, v/v). After rotary evaporation GSLs were taken up in a defined volume of chloroform/methanol (2/1, v/v) equivalent to 1×10^4 cells/μL and stored at −20°C until use.

GSL references and standard PLs

A preparation of neutral GSLs from human erythrocytes, harboring Gb3Cer (Galα4Galβ4Glcβ1Cer) and Gb4Cer (GalNAcβ3Galα4Galβ4Glcβ1Cer), served as reference (R1) and positive control for the TLC overlay assays (Meisen et al. 2005; Souady et al. 2009). The nomenclature of the GSLs follows the IUPAC-IUB recommendations 1997 (Chester 1998). The employed reference mixture of PLs (R2) was composed of cardiolipin (CL), phosphatidylglycerol (PG) , PE, phosphatidic acid (PA), lyso-PE, PC and SM as previously described (Kouzel et al. 2013; Meisen et al. 2013).

Anti-Stx, anti-flotillin-2, anti-GSL and secondary antibodies

The monoclonal mouse IgG-antibodies against Stx1a (clone VT109/4-E9) and Stx2a (clone VT135/6-B9) were purchased from SIFIN GmbH (Berlin, Germany) (Schweppe et al. 2010; Storck et al. 2012). The monoclonal rabbit anti-flotillin-2 antibody (C42A3, Cat. No. 3436) was from Cell Signaling Technology, Inc. (Danvers, MA, USA) (Betz et al. 2011). The specificities of polyclonal chicken IgY antibodies against Gb3Cer and Gb4Cer have been described in previous publications (Meisen et al. 2005; Distler et al. 2009; Hoffmann et al. 2010; Schweppe et al. 2010). Alkaline phosphatase (AP)-conjugated goat anti-mouse IgG (Code 115055-003), goat anti-rabbit IgG (Code 111055-003), and rabbit anti-chicken IgY (Code 303055-033) secondary antibodies were from Dianova (Hamburg, Germany).

High-performance TLC and staining of GSLs and PLs

GSLs and PLs were applied onto silica gel 60 precoated glass plates (HPTLC plates, size 10 cm × 10 cm, thickness 0.2 mm, no. 1.05633.0001; Merck, Darmstadt, Germany) with an automatic sample applicator (Linomat IV, CAMAG, Muttenz, Switzerland). GSLs were separated in chloroform/methanol/water (120/70/17, each by vol.) and stained with orcinol (Müthing 1998). PLs were chromatographed in chloroform/methanol/isopropanol/triethylamine/0.25% aqueous KCl (30/9/25/18/6, each by volume) and stained with molybdenum blue Dittmer-Lester reagent (Dittmer and Lester 1964; Müthing and Radloff 1998).

TLC overlay assay of GSLs

Polyclonal chicken anti-GSL antibodies specific for Gb3Cer and Gb4Cer as well as Stx1a and Stx2a were employed for the

detection of Stx receptors in GSL preparations of pHBMECs according to protocols published previously (Schweppe et al. 2010; Betz et al. 2011; Storck et al. 2012; Kouzel et al. 2013; Steil et al. 2015). Briefly, upon TLC separation the silica gel of the glass plate was at first fixed with 0.5% (w/v) polyisobutylmethacrylate (Plexigum P28, Röhm, Darmstadt, Germany) solution. TLC overlay assay immunodetection was done with primary anti-Gb3Cer and anti-Gb4Cer antibodies combined with secondary AP-conjugated anti-chicken IgY antibodies (both in 1:2000 dilutions). Alternatively, TLC plates were overlayed with Stx1a or Stx2a (0.2 µg/mL each), followed by incubation of the chromatogram with anti-Stx1 or anti-Stx2 antibodies (1:1000 dilution each) and AP-conjugated secondary anti-mouse IgG-antibodies (diluted 1:2000). Bound antibodies were visualized with 0.05% (w/v) enzyme substrate 5-bromo-4-chloro-3-indolyl phosphate *p*-toluidine salt (BCIP, Roth, Karlsruhe, Germany) in glycine buffer (Müthing 1998). Immunostained GSLs were quantified densitometrically using a CD60 scanner (Desaga, Heidelberg, Germany, software ProQuant®, version 1.06.000) in reflectance mode with a light beam slit of 0.02 mm × 4 mm at a wavelength of $\lambda = 630$ nm (Betz et al. 2011; Kouzel et al. 2013; Meisen et al. 2013; Steil et al. 2015).

Preparation of DRM and nonDRM fractions from sucrose density gradients

Sucrose density gradient fractions were prepared following the original description of Brown and Rose (Brown and Rose 1992) with minor modifications as previously described (Betz et al. 2011; Kouzel et al. 2013; Meisen et al. 2013; Steil et al. 2015). In short, confluent grown pHBMECs were disintegrated in lysis buffer followed by removal of cell debris by gentle centrifugation (400 × *g*) and separation of membranes from cytosol by short ultracentrifugation (150,000 × *g*) of the supernatant. The membrane sediment was solubilized in 1% Triton X-100 buffer and mixed in equal ratios with 85% sucrose. The 42.5% sucrose solution was then overlayed with a discontinuous sucrose gradient of 30% and 5% sucrose. Eight fractions of 1.5 mL each were collected from the gradient, namely three top DRM-associated fractions (F1–F3) and five nonDRM fractions (F4–F8), obtained by ultracentrifugation (200,000 × *g*).

Isolation of proteins, GSLs and PLs from gradient fractions

For protein analysis, 0.3 mL of each sucrose gradient fraction was dialyzed at 4°C for 2 days against distilled water to remove sucrose and freeze dried. Proteins were precipitated with 5% (w/v) trichloroacetic acid, washed with absolute ethanol, and applied to SDS-PAGE followed by Western blotting (Betz et al. 2011). For PL analysis, 0.5 mL of each fraction was dialyzed, freeze dried, solubilized under short sonication in chloroform/methanol (2/1, v/v) and adjusted to defined volumes corresponding to 1×10^5 cells/µL. For GSL analysis, 0.5 mL of each fraction was submitted to 1 N NaOH alkaline treatment for 1 h at 37°C under gentle rotation to saponify glycerophospholipids and TGs, followed by neutralization with HCl (Kouzel et al. 2013). After dialysis and freeze drying the extracts were dissolved in chloroform/methanol (2/1, v/v) and adjusted to a concentration corresponding to 1×10^5 cells/µL.

SDS-PAGE and Western blotting

Proteins of sucrose gradient fractions were precipitated and electrophoresed as previously described (Betz et al. 2011; Kouzel et al. 2013). After semi-dry blotting onto nitrocellulose the membrane was overlayed with anti-flotillin-2 antibody (1:4000 dilution) and then incubated with AP-conjugated anti-rabbit IgG secondary antibody (1:2000 dilution). Detection of bound antibodies was performed with nitroblue tetrazolium/BCIP kit (Invitrogen).

Mass spectrometry

Electrospray ionization mass spectrometry (ESI MS) was performed by use of a quadrupole time-of-flight mass spectrometer equipped with a nanospray manipulator (Micromass, Manchester, UK) in the positive ion mode as described previously (Hoffmann et al. 2010; Schweppe et al. 2010; Müthing et al. 2012). For MS^1 spectra aliquots of lipid extracts were dried under a stream of nitrogen and dissolved in methanol containing 1% (v/v) formic acid. Assignment of proposed structures of PL and GSL analytes was confirmed by use of low energy collision-induced dissociation experiments (MS^2). For MS^2 experiments, precursor ions were selected in the quadrupole analyser and fragmented in the collision cell using a collision gas (Ar) pressure of 3.0×10^{-3} Pa and collision energies of 20–40 eV (E_{lab}).

Supplementary data

Supplementary data for this article are available online at http://glycob.oxfordjournals.org/.

Funding

This work was supported by grants from the German Research Foundation (DFG, grant number MU845/4-2) and the German Federal Ministry of Education and Research (BMBF), conducted under the umbrella of the German Center for Infection Research (DZIF, TTU 06.801) with assistance of InfectControl 2020 (TFP-TV8-AS12).

Acknowledgements

The expert technical assistance of Dagmar Mense and Nikola Skutta is gratefully acknowledged. We thank Dr. Iris Meisen for the two spectra of Gb3Cer and Gb4Cer from total GSL preparations, Dr. Michael Mormann for use of the quadrupole time-of-flight mass spectrometer and Björn Weege for help with glycosphingolipid analysis.

Conflict of interest statement

None declared.

Abbreviations

DRM(s), detergent-resistant membrane(s); EHEC, enterohemorrhagic *Escherichia coli*; Gb3Cer, globotriaosylceramide; Gb4Cer, globotetraosylceramide; GSL(s), glycosphingolipid(s); HUS, hemolytic-uremic syndrome; PC, phosphatidylcholine; PE, phosphatidylethanolamine; pHBMECs, primary human brain microvascular endothelial cells; PL(s), phospholipid(s); SM, sphingomyelin; STEC, Stx-producing *Escherichia coli*; Stx, Shiga toxin; TTP, thrombotic thrombocytopenic purpura.

References

Barras A, Martin FA, Bande O, Baumann JS, Ghigo JM, Boukherroub R, Beloin C, Siriwardena A, Szunerits S. 2013. Glycan-functionalized

diamond nanoparticles as potent *E. coli* anti-adhesives. *Nanoscale*. 5: 2307–2316.

Bauwens A, Bielaszewska M, Kemper B, Langehanenberg P, von Bally G, Reichelt R, Mulac D, Humpf HU, Friedrich AW, Kim KS, et al. 2011. Differential cytotoxic actions of Shiga toxin 1 and Shiga toxin 2 on microvascular and macrovascular endothelial cells. *Thromb Haemost*. 105:515–528.

Bauwens A, Betz J, Meisen I, Kemper B, Karch H, Müthing J. 2013. Facing glycosphingolipid-Shiga toxin interaction: Dire straits for endothelial cells of the human vasculature. *Cell Mol Life Sci*. 70:425–457.

Betz J, Bielaszewska M, Thies A, Humpf HU, Dreisewerd K, Karch H, Kim KS, Friedrich AW, Müthing J. 2011. Shiga toxin glycosphingolipid receptors in microvascular and macrovascular endothelial cells: Differential association with membrane lipid raft microdomains. *J Lipid Res*. 52:618–634.

Betz J, Dorn I, Kouzel IU, Bauwens A, Meisen I, Kemper B, Bielaszewska M, Mormann M, Weymann L, Sibrowski W, et al. 2016. Shiga toxin of enterohaemorrhagic *Escherichia coli* directly injures developing human erythrocytes. *Cell Microbiol*. doi:10.1111/cmi.12592.

Bielaszewska M, Karch H. 2005. Consequences of enterohaemorrhagic *Escherichia coli* infection for the vascular endothelium. *Thromb Haemost*. 94:312–318.

Brigotti M, Alfieri R, Sestili P, Bonelli M, Petronini PG, Guidarelli A, Barbieri L, Stirpe F, Sperti S. 2002. Damage to nuclear DNA induced by Shiga toxin 1 and ricin in human endothelial cells. *FASEB J*. 16:365–372.

Brigotti M, Carnicelli D, Arfilli V, Tamassia N, Borsetti F, Fabbri E, Tazzari PL, Ricci F, Pagliaro P, Spisni E, et al. 2013. Identification of TLR4 as the receptor that recognizes Shiga toxin in human neutrophils. *J Immunol*. 191:4748–4758.

Brown DA, Rose JK. 1992. Sorting of GPI-anchored proteins to glycolipid-enriched membrane subdomains during transport to the apical cell surface. *Cell*. 68:533–544.

Brown DA. 2006. Lipid rafts, detergent-resistant membranes, and raft targeting signals. *Physiology*. 21:430–439.

Carnicelli D, Arfilli V, Ricci F, Velati C, Tazzari PL, Brigotti M. 2016. The antibiotic polymyxin B impairs the interactions between Shiga toxins and human neutrophils. *J Immunol*. 196:1177–1185.

Carquin M, D'Auria L, Pollet H, Bongarzone ER, Tyteca D. 2015. Recent progress on lipid lateral heterogeneity in plasma membranes: From rafts to submicrometric domains. *Prog Lipid Res*. 62:1–24.

Chester MA. 1998. IUPAC-IUB Joint Commission on Biochemical Nomenclature (JCBN). Nomenclature of glycolipids-recommendations 1997. *Eur J Biochem*. 257:293–298.

Chien YY, Jan MD, Adak AK, Tzeng HC, Lin YP, Chen YJ, Wang KT, Chen CT, Chen CC, Lin CC. 2008. Globotriose-functionalized gold nanoparticles as multivalent probes for Shiga-like toxin. *ChemBioChem*. 9: 1100–1109.

Chinnapen DJ, Chinnapen H, Saslowsky S, Lencer WI. 2007. Rafting with cholera toxin: Endocytosis and trafficking from plasma membrane to ER. *FEMS Microbiol Lett*. 266:129–137.

Ciana A, Achilli C, Minetti G. 2014. Membrane rafts of the human red blood cell. *Mol Membr Biol*. 31:47–57.

Cooling LL, Walker KE, Gille T, Koerner TA. 1998. Shiga toxin binds to human platelets via globotriaosylceramide (P^k antigen) and a novel platelet glycosphingolipid. *Infect Immun*. 66:4355–4366.

Distler U, Souady J, Hülsewig M, Drmić-Hofman I, Haier J, Friedrich AW, Karch H, Senninger N, Dreisewerd K, Berkenkamp S, et al. 2009. Shiga toxin receptor Gb3Cer/CD77: Tumor association and promising therapeutic target in pancreas and colon cancer. *PLoS One*. 4:e6813.

Dittmer JC, Lester RL. 1964. A simple, specific spray for the detection of phospholipids on thin-layer chromatograms. *J Lipid Res*. 15:126–127.

Domon B, Costello CE. 1988a. Structure elucidation of glycosphingolipids and gangliosides using high-performance tandem mass spectrometry. *Biochemistry*. 27:1534–1543.

Domon B, Costello CE. 1988b. A systematic nomenclature for carbohydrate fragmentation in FAB-MS/MS spectra of glycoconjugates. *Glycoconj J*. 5: 397–409.

Eisenhauer PB, Chaturvedi P, Fine RE, Ritchie AJ, Pober JS, Cleary TG, Newburg DS. 2001. Tumor necrosis factor alpha increases human cerebral endothelial cell Gb_3 and sensitivity to Shiga toxin. *Infect Immun*. 69: 1889–1894.

Eisenhauer PB, Jacewicz MS, Conn KJ, Koul O, Wells JM, Fine RE, Newburg DS. 2004. *Escherichia coli* Shiga toxin 1 and TNF-alpha induce cytokine release by human cerebral microvascular endothelial cells. *Microb Pathog*. 36:189–196.

Ergonul Z, Hughes AK, Kohan DE. 2003. Induction of apoptosis of human brain microvascular endothelial cells by Shiga toxin 1. *J Infect Dis*. 187: 154–158.

Fujinaga Y, Wolf AA, Rodighiero C, Wheeler H, Tsai B, Allen L, Jobling MG, Rapoport T, Holmes RK, Lencer WI. 2003. Gangliosides that associate with lipid rafts mediate transport of cholera and related toxins from the plasma membrane to endoplasmic reticulum. *Mol Biol Cell*. 14:4783–4793.

Ghosh SA, Polanowska-Grabowska RK, Fujii J, Obrig T, Gear AR. 2004. Shiga toxin binds to activated platelets. *J Thromb Haemost*. 2:499–506.

Gupta G, Surolia A. 2010. Glycosphingolipids in microdomain formation and their spatial organization. *FEBS Lett*. 584:1634–1641.

Hanada K. 2005. Sphingolipids in infectious diseases. *Jpn J Infect Dis*. 58: 131–148.

Head BP, Patel HH, Insel PA. 2014. Interaction of membrane/lipid rafts with the cytoskeleton: Impact on signaling and function: Membrane/lipid rafts, mediators of cytoskeletal arrangement and cell signaling. *Biochim Biophys Acta*. 1838:532–545.

Hoffmann P, Hülsewig M, Duvar S, Ziehr H, Mormann M, Peter-Katalinić J, Friedrich AW, Karch H, Müthing J. 2010. On the structural diversity of Shiga toxin glycosphingolipid receptors in lymphoid and myeloid cells determined by nanoelectrospray ionization tandem mass spectrometry. *Rapid Commun Mass Spectrom*. 24:2295–2304.

Jansson L, Ångström J, Lebens M, Imberty A, Varrot A, Tenebrg S. 2010. Carbohydrate binding specificities and crystal structure of the cholera toxin-like B-subunit from *Citrobacter freundii*. *Biochimie*. 92:482–490.

Kanda T, Ariga T, Kubodera H, Jin HL, Owada K, Kasama T, Yamawaki M, Mizusawa H. 2004. Glycosphingolipid composition of primary cultured human brain microvsacular endothelial cells. *J Neurosci Res*. 78: 141–150.

Karch H, Tarr PI, Bielaszewska M. 2005. Enterohaemorrhagic *Escherichia coli* in human medicine. *Int J Med Microbiol*. 295:405–418.

Karlsson KA. 1995. Microbial recognition of target-cell glycoconjugates. *Curr Opin Struct Biol*. 5:622–635.

Khan F, Proulx F, Lingwood CA. 2009. Detergent-resistant globotriaosyl ceramide may define verotoxin/glomeruli-restricted haemolytic uremic syndrome pathology. *Kidney Int*. 75:1209–1216.

Klotzsch E, Schütz GJ. 2013. A critical survey of methods to detect plasma membrane rafts. *Philos Trans R Soc Lond B Biol Sci*. 368:20120033.

Komura N, Suzuki KGN, Ando H, Konishi M, Koikeda M, Imamura A, Chadda R, Fujiwara TK, Tsuboi H, Sheng R, et al. 2016. Raft-based interactions of gangliosides with a GPI-anchored receptor. *Nat Chem Biol*. 12:402–410.

Kouzel IU, Pohlentz G, Storck W, Radamm L, Hoffmann P, Bielaszewska M, Bauwens A, Cichon C, Schmidt AM, Mormann M, et al. 2013. Association of Shiga toxin glycosphingolipid receptors with membrane microdomains of toxin-sensitive lymphoid and myeloid cells. *J Lipid Res*. 54:692–710.

Lencer WI, Saslowsky D. 2005. Raft trafficking of AB_5 subunit bacterial toxins. *Biochim Biophys Acta*. 1746:314–321.

Levery SB. 2005. Glycosphingolipid structural analysis and glycosphingolipidomics. *Methods Enzymol*. 405:300–369.

Lingwood CA, Binnington B, Manis A, Branch DR. 2010. Globotriaosyl ceramide receptor function—Where membrane structure and pathology intersect. *FEBS Lett*. 584:1879–1886.

Lingwood D, Simons K. 2007. Detergent resistance as a tool in membrane research. *Nat Protoc*. 2:2159–2165.

Lingwood D, Simons K. 2010. Lipid rafts as a membrane-organizing principle. *Science*. 327:46–50.

Meisen I, Friedrich AW, Karch H, Witting U, Peter-Katalinić J, Müthing J. 2005. Application of combined high-performance thin-layer chromatography immunostaining and nanoelectrospray ionization quadrupole time-of-flight tandem mass spectrometry to the structural characterization of high- and low-affinity binding ligands of Shiga toxin 1. *Rapid Commun Mass Spectrom*. 19:3659–3665.

Meisen I, Mormann M, Müthing J. 2011. Thin-layer chromatography, overlay technique and mass spectrometry: A versatile triad advancing glycosphingolipidomics. *Biochim Biophys Acta*. 1811:875–896.

Meisen I, Rosenbrück R, Galla HJ, Hüwel S, Kouzel IU, Mormann M, Karch H, Müthing J. 2013. Expression of Shiga toxin 2e glycosphingolipid receptors of primary porcine brain endothelial cells and toxin-mediated breakdown of the blood-brain barrier. *Glycobiology*. 23:745–759.

Mochalin VN, Shenderova O, Ho D, Gogotsi Y. 2012. The properties and applications of nanodiamonds. *Nat Nanotechnol*.. 7:11–23.

Morris RJ, Jen A, Warley A. 2011. Isolation of nano-meso scale detergent resistant membrane that has properties expected of lipid 'rafts'. *J Neurochem*. 116:671–677.

Müthing J. 1998. TLC in structure and recognition studies of glycosphingolipids. In: Hounsell EF, editor. *Methods in molecular biology* Totowa, NJ, USA, Humana Press Inc. p.183–195.

Müthing J, Radloff M. 1998. Nanogram detection of phospholipids on thin-layer chromatograms. *Anal Biochem*. 257:67–70.

Müthing J, Schweppe CH, Karch H, Friedrich AW. 2009. Shiga toxins, glycosphingolipid diversity, and endothelial cell injury. *Thromb Haemost*. 101: 252–264.

Müthing J, Distler U. 2010. Advances on the compositional analysis of glycosphingolipids combining thin-layer chromatography with mass spectrometry. *Mass Spectrom Rev*. 29:425–479.

Müthing J, Meisen I, Zhang W, Bielaszewska M, Mormann M, Bauerfeind R, Schmidt MA, Friedrich AW, Karch H. 2012. Promiscuous Shiga toxin 2e and its intimate relationship to Forssman. *Glycobiology*. 22:849–862.

Nangaku M, Nishi H, Fujita T. 2007. Pathogenesis and progress of thrombotic microangiopathy. *Clin Exp Nephrol*. 11:107–114.

Obrig TG, Karpman D. 2012. Shiga toxin pathogenesis: Kidney complications and renal failure. *Curr Top Microbiol Immunol*. 357:105–136.

Porubsky S, Federico G, Müthing J, Jennemann R, Gretz N, Büttner S, Obermüller N, Jung O, Hauser IA, Gröne E, et al. 2014. Direct acute tubular damage contributes to Shigatoxin-mediated kidney failure. *J Pathol*. 234:120–133.

Prinetti A, Loberto N, Chigorno V, Sonnino S. 2009. Glycosphingolipid behaviour in complex membranes. *Biochim Biophys Acta*. 1788:184–193.

Ramegowda B, Samuel JE, Tesh VL. 1999. Interaction of Shiga toxins with human brain microvascular endothelial cells: Cytokines as sensitizing agents. *J Infect Dis*. 180:1205–1213.

Richards A, Kavanagh D. 2009. Pathogenesis and thrombotic microangiopathy: Insights from animal models. *Nephron Exp Nephrol*. 113:e97–e103.

Róg T, Vattulainen I. 2014. Cholesterol, sphingolipids, and glycolipids: What do we know about their role in raft-like membranes? *Chem Phys Lipids*. 184:82–104.

Sandvig K, Bergan J, Dyve AB, Skotland T, Torgersen ML. 2010. Endocytosis and retrograde transport of Shiga toxin. *Toxicon*. 56:1181–1185.

Scheutz F, Teel LD, Beutin L, Piérard D, Buvens G, Karch H, Mellmann A, Caprioli A, Tozzoli R, Morabito S, et al. 2012. Multicenter evaluation of a sequence-based protocol for subtyping Shiga toxins and standardizing Stxs nomenclature. *J Clin Microbiol*. 50:2951–2963.

Schweppe CH, Bielaszewska M, Pohlentz G, Friedrich AW, Büntemeyer H, Schmidt MA, Kim KS, Peter-Katalinić J, Karch H, Müthing J. 2008. Glycosphingolipids in vascular endothelial cells: Relationship of heterogeneity in Gb3Cer/CD77 receptor expression with differential Shiga toxin 1 cytotoxicity. *Glycoconj J*. 25:291–304.

Schweppe CH, Hoffmann P, Nofer JR, Pohlentz G, Mormann M, Karch H, Friedrich AW, Müthing J. 2010. Neutral glycosphingolipids in human blood: A precise mass spectrometry analysis with special reference to lipoprotein-associated Shiga toxin receptors. *J Lipid Res*. 51:2282–2294.

Sestili P, Alfieri R, Carnicelli D, Martinelli C, Barbieri L, Stirpe F, Bonelli M, Petronini PG, Brigotti M. 2005. Shiga toxin 1 and ricin inhibit the repair of H_2O_2-induced DNA single strand breaks in cultured mammalian cells. *DNA Repair*. 4:271–277.

Sharon N. 2006. Carbohydrates as future anti-adhesion drugs for infectious diseases. *Biochim Biophys Acta*. 1760:527–537.

Simons K, Gerl MJ. 2010. Revitalizing membrane rafts: New tools and insights. *Nat Rev Mol Cell Biol*. 11:688–699.

Smith HW, Linggood MA. 1971. The transmissible nature of enterotoxin production in human enteropathogenic strain of *Escherichia coli*. *J Med Microbiol*. 4:301–305.

Smith DC, Lord JM, Roberts LM, Johannes L. 2004. Glycosphingolipids as toxin receptors. *Semin Cell Dev Biol*. 15:397–408.

Smith DC, Sillence DJ, Falguières T, Jarvis RM, Johannes L, Lord JM, Platt FM, Roberts LM. 2006. The association of Shiga-like toxin with detergent-resistant membranes is modulated by glucosylceramide and is an essential requirement in the endoplasmic reticulum for a cytotoxic effect. *Mol Biol Cell*. 17:1375–1387.

Sonnino S, Aureli M, Mauri L, Ciampa MG, Prinetti A. 2015. Membrane lipid domains in the nervous system. *Front Biosci (Landmar Ed)*. 20:280–302.

Souady J, Soltwisch J, Dreisewerd K, Haier J, Peter-Katalinić J, Müthing J. 2009. Structural profiling of individual glycosphingolipids in a single thin-layer chromatogram by multiple sequential immunodetection matched with direct IR-MALDI-o-TOF mass spectrometry. *Anal Chem*. 81:9481–9492.

Steil D, Schepers CL, Pohlentz G, Legros N, Runde J, Humpf HU, Karch H, Müthing J. 2015. Shiga toxin glycosphingolipid receptors of Vero-B4 kidney epithelial cells and their membrane microdomain lipid environment. *J Lipid Res*. 56:2322–2336.

Storck W, Meisen I, Gianmoena K, Pläger I, Kouzel IU, Bielaszewska M, Haier J, Mormann M, Humpf HU, Karch H, et al. 2012. Shiga toxin glycosphingolipid receptor expression and toxin susceptibility of human pancreatic ductal adenocarcinomas of differing origin and differentiation. *Biol Chem*. 393:785–799.

Stricklett PK, Hughes AK, Ergonul Z, Kohan DE. 2002. Molecular basis for up-regulation by inflammatory cytokines of Shiga toxin 1 cytotoxicity and globotriaosylceramide expression. *J Infect Dis*. 186:976–982.

Strockbine NA, Marques LR, Newland JW, Smith HW, Holmes RK, O'Brien AD. 1986. Two toxin-converting phages from *Escherichia coli* O157:H7 strain 933 encode antigenically distinct toxins with similar biologic activities. *Infect Immun*. 53:135–140.

Tarr PI, Gordon CA, Chandler WL. 2005. Shiga-toxin-producing *Escherichia coli* and haemolytic uraemic syndrome. *Lancet*. 365:1073–1086.

Teneberg S, Ångström J, Ljungh A. 2004. Carbohydrate recognition by enterohemorrhagic *Escherichia coli*: Characterization of a novel glycosphingolipid from cat small intestine. *Glycobiology*. 14:187–196.

Trachtman H, Austin C, Lewinski M, Stahl RA. 2012. Renal and neurological involvement in typical Shiga toxin-associated HUS. *Nat Rev Nephrol*. 8:658–669.

Tsai HM. 2006. The molecular biology of thrombotic microangiopathy. *Kidney Int*. 70:16–23.

Vieira FS, Corrêa G, Einicker-Lamas M, Coutinho-Silva R. 2010. Host-cell lipid rafts: A safe door for micro-organisms? *Biol Cell*. 102:391–407.

Zheng XL, Sadler JE. 2008. Pathogenesis of thrombotic microangiopathies. *Annu Rev Pathol*. 3:249–277.

Zoja C, Buelli S, Morigi M. 2010. Shiga toxin-associated hemolytic uremic syndrome: Pathophysiology of endothelial dysfunction. *Pediatr Nephrol*. 25:2231–2240.